NANO LETTERS

Letter

pubs.acs.org/NanoLett

Adhesive Nanoparticles as Local Probes of Membrane Curvature

Jaime Agudo-Canalejo and Reinhard Lipowsky*

Theory and Bio-Systems, Max Planck Institute of Colloids and Interfaces, 14424 Potsdam, Germany

ABSTRACT: Biological and biomimetic membranes display complex shapes with nonuniform curvature. Because the interaction of adhesive nanoparticles with such membranes depends on the local membrane curvature, different segments of the same membrane can differ in their engulfment behavior. For a single vesicle in contact with many nanoparticles, we predict ten distinct engulfment patterns as well as morphological transitions between these patterns, which are directly accessible to experiment.

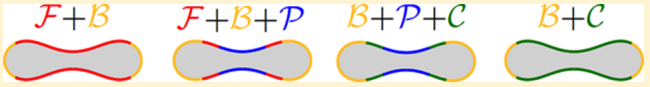

KEYWORDS: *membranes and vesicles, nanoparticle−membrane adhesion, nanoparticle engulfment, bilayer asymmetry, local stability analysis, contact mean curvature, spontaneous curvature*

Nanoparticles are widely used to deliver drugs, imaging agents, and toxins to biological cells.[1,2] The cellular uptake of a nanoparticle requires the engulfment of this particle by the cell membrane, a process that is dominated by the competition between particle adhesion and membrane bending.[3] The underlying interactions can be studied experimentally in biomimetic systems consisting of nanoparticles and lipid[4−8] or polymer[9] vesicles. Several theoretical and computational methods have also been used to elucidate the engulfment process.[10−18] However, all of these previous studies of nanoparticle−membrane systems have ignored one important aspect of biological and biomimetic membranes, namely their complex, nontrivial shapes.[19−22] Cells and cellular organelles display a whole catalogue of shapes, such as the prolate-like shapes of dividing cells or mitochondria; the discocyte, stomatocyte, and echinocyte shapes of red blood cells; the invaginated, stomatocyte-like shapes of nascent autophagosomes; or the recently reported "parking garage" shapes of the endoplasmic reticulum.[23] Interestingly, many of these shapes can be mimicked using lipid[19] or polymer vesicles.[24] In particular, prolate, discocyte, and stomatocyte shapes arise naturally as the shapes that minimize the bending energy of closed vesicle membranes with constrained volume[20] and will be used as examples of complex membrane shapes in the following. Our results also apply to vesicle shapes that are topologically distinct from a sphere, corresponding to toroidal or higher genus shapes with one or several handles.[25,26]

Previous theoretical studies of nanoparticle−membrane systems have been subject to certain limitations. Direct computation of minimal energy shapes of membranes is only possible for axisymmetric geometries, and therefore, previous work has been restricted to the engulfment of spherical particles by planar membranes[10,12] or at the poles of closed axisymmetric vesicles.[11,13,14] The study of nonaxisymmetric geometries is computationally expensive because it requires the numerical energy minimization of triangulated or spline surfaces,[15,16] or alternatively molecular dynamics simulations,[17,18] and efforts have focused mainly on the engulfment of nonspherical particles by planar membranes. In this Letter, we show how the approach introduced in ref 14, based on local stability analysis of free and completely engulfed particles, can be used to understand the engulfment of spherical particles at nonaxisymmetric locations on the vesicle surface. In this way, we can elucidate the interaction of nanoparticles with membranes of any shape.

In general, attractive interactions between a nanoparticle and a membrane can lead to different states of engulfment. Previous studies have shown that spherical nanoparticles do not bind to membranes for weak attractive interactions but become completely engulfed for sufficiently strong adhesion.[3,10] Recently, we found[14] that concave membrane segments with negative mean curvature stabilize partially engulfed states, in which the membrane covers only a fraction of the particle surface, whereas convex segments with positive mean curvature favor bistability of unbound and completely engulfed particles. We thus identified four distinct stability regimes for the nanoparticles and the associated membrane segments: free $\mathcal{F}$ segments do not bind the particles at all; $\mathcal{C}$ segments completely engulf the particles, whereas $\mathcal{P}$ segments engulf them only partially; finally, bistable $\mathcal{B}$ segments exhibit an energy barrier between free and completely engulfed particles.

Each type of membrane segment is stable over a certain range of mean curvatures. As a consequence, the different types of segments can coexist on a single vesicle, creating engulfment patterns with many nanoparticles when the vesicle is exposed to a solution of such particles; see Figure 1. We predict that a single vesicle can exhibit ten distinct engulfment patterns: four single-segment patterns, with the whole vesicle membrane being composed of a single $\mathcal{F}$, $\mathcal{P}$, $\mathcal{C}$, or $\mathcal{B}$ segment, four two-segment patterns, namely $\mathcal{F}+\mathcal{B}$, $\mathcal{B}+\mathcal{C}$, $\mathcal{F}+\mathcal{P}$, or $\mathcal{P}+\mathcal{C}$, and two three-segment patterns provided by $\mathcal{F}+\mathcal{B}+\mathcal{P}$ or $\mathcal{B}+\mathcal{P}+\mathcal{C}$. Which pattern is present depends on three parameters: the spontaneous curvature of the membrane, the reduced volume of the vesicle, which controls its overall shape, and the

Received: August 28, 2015
Revised: September 29, 2015
Published: October 2, 2015

DOI: 10.1021/acs.nanolett.5b03475
Nano Lett. 2015, 15, 7168−7173

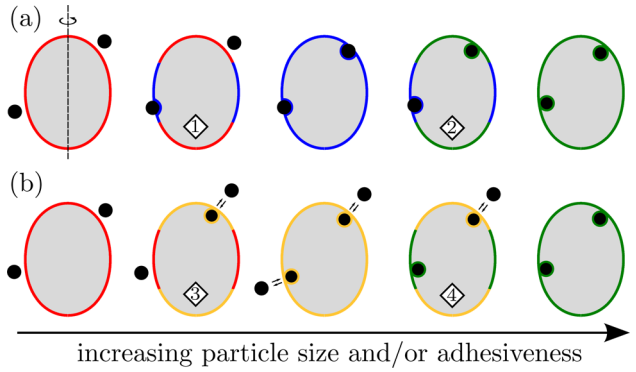

Figure 1. Different engulfment patterns of nanoparticles (black) on a prolate vesicle. The spontaneous curvature of the vesicle membrane is positive in (a) and negative in (b). The patterns involve four types of membrane segments: free segments with no engulfment (red) and bistable segments with activated engulfment and release (yellowish orange) as well as segments decorated by partially engulfed (blue) and completely engulfed (green) particles. A change in particle size or adhesiveness leads to continuous morphological transitions between these patterns. The numbered diamonds refer to Figure 3, below.

contact mean curvature, which encodes the information on the size and adhesiveness of the nanoparticles. All three parameters can be controlled experimentally, and changes in these parameters lead to continuous morphological transitions between the different patterns.

Our Letter is organized as follows. We first focus on endocytic engulfment of particles originating from the *exterior* aqueous compartment and briefly review how the stability of free and completely engulfed particles leads to four stability regimes for a single particle.[14] We then show how, for sufficiently small nanoparticles, these stability regimes depend on only three parameters that also determine the possible engulfment patterns. Next, we extend our theory to exocytic engulfment of particles originating from the *interior* aqueous compartment and argue that membrane-mediated interactions between the particles do not affect the engulfment patterns. Finally, we discuss the engulfment patterns in connection to experiments.

Engulfment can be understood from the interplay between particle adhesion and membrane bending. According to the spontaneous curvature model,[20,27] the bending energy density of the membrane is given by $\mathcal{E}_{be} = 2\kappa(M - m)^2$, where M is the mean curvature, which typically varies along the vesicle membrane. The relevant material parameters of the membrane are its bending rigidity κ and its spontaneous curvature m. The attractive interaction with the particle is described by the adhesive strength, $|W|$, which represents the absolute value of the adhesive free energy per unit area.[28] We first focus on endocytic engulfment of rigid spherical particles with radius R_{pa} by a vesicle with total membrane area A and enclosed volume V. These three geometrical parameters, together with the three material parameters κ, m, and $|W|$, determine the particle–vesicle morphologies. It will be useful to define the *contact mean curvature*

$$M_{co} \equiv \frac{1}{R_{pa}}\left(\sqrt{\frac{|W|R_{pa}^2}{2\kappa}} - 1\right) \tag{1}$$

which encodes the competition between adhesion and bending into a single length scale, and represents[14] the equilibrium mean curvature of the membrane along the contact line with the adhering particle. It is important to note that the contact mean curvature increases both with increasing particle size and with increasing adhesive strength.

Let us consider a small segment of the vesicle membrane with mean curvature M_{ms}. The stability limit L_{fr} of a free particle coming into contact with this segment is given by the relation

$$M_{co} = M_{ms} \tag{2}$$

between the contact mean curvature M_{co} and the mean curvature M_{ms} of the unperturbed membrane segment. The free state is stable for large segment curvatures with $M_{ms} > M_{co}$ but is unstable for small segment curvatures with $M_{ms} < M_{co}$.

In the completely engulfed state, the particle is fully covered by the membrane but is still connected to the mother vesicle by a narrow membrane neck. In the continuum approach used here, the completely engulfed state represents a limit shape with an ideal neck that is attached to the mother vesicle at a single contact point. If the mean curvature of the mother vesicle at this contact point is denoted by M'_{ms}, the stability limit L_{ce} of the completely engulfed particle is given by

$$M_{co} + M'_{ms} = 2m \tag{3}$$

The completely engulfed state is stable if the mother segment curvature is large and satisfies $M'_{ms} > 2m - M_{co}$ but unstable if it is small with $M'_{ms} < 2m - M_{co}$.

Equations 2 and 3 were validated in ref 14 via extensive numerical calculations and detailed theoretical considerations. We also found that, in the case of particles much smaller than the vesicle, a partially engulfed state can only be stable if both the free and the completely engulfed state are unstable. The two relations in eqs 2 and 3 then define the boundaries of four stability regimes for the nanoparticles and the associated membrane segments: (i) For $M_{ms} > M_{co}$ and $M'_{ms} < 2m - M_{co}$, the free state is stable and the completely engulfed state is unstable, which defines a stable $\mathcal{F}$ segment; (ii) for $M_{ms} > M_{co}$ and $M'_{ms} > 2m - M_{co}$, both the free and the completely engulfed state are stable and the segment belongs to a bistable $\mathcal{B}$ segment; (iii) for $M_{ms} < M_{co}$ and $M'_{ms} > 2m - M_{co}$, the free state is unstable and the completely engulfed state is stable, which implies a stable C segment; and (iv) for $M_{ms} < M_{co}$ and $M'_{ms} < 2m - M_{co}$, both the free and the completely engulfed state are unstable, and the particle should be partially engulfed by the membrane segment, which then belongs to a stable $\mathcal{P}$ segment.

Vesicle membranes divide the aqueous phase into an interior and exterior compartment. When both compartments contain osmotically active agents, the vesicle adapts its volume in such a way that the osmotic pressure in the interior compartment balances the exterior osmotic pressure. The equilibrium shapes of such a vesicle with volume V, membrane area A, and vesicle size $R_{ve} \equiv \sqrt{A/4\pi}$ are then determined, in the absence of nanoparticles, by the reduced volume $v \equiv 3V/4\pi R_{ve}^3$ and the spontaneous curvature m.[20] In general, these equilibrium shapes form several stable branches such as the prolate and oblate branches for $0.65 \lesssim v < 1$ and $m = 0$. When a vesicle with area A and volume V completely engulfs N_{pa} nanoparticles, its overall shape is determined by the decreased area $A - 4\pi R_{pa}^2 N_{pa}$ and the increased volume $V + (4\pi/3)R_{pa}^3 N_{pa}$. Therefore, the reduced overall volume is increased from v to

DOI: 10.1021/acs.nanolett.5b03475
Nano Lett. 2015, 15, 7168–7173

$$v' = \frac{v + N_{pa}(R_{pa}/R_{ve})^3}{[1 - N_{pa}(R_{pa}/R_{ve})^2]^{3/2}} \approx v\left[1 + \frac{3N_{pa}}{2}\left(\frac{R_{pa}}{R_{ve}}\right)^2\right] \quad (4)$$

where the asymptotic equality holds for small particle radii $R_{pa} \ll R_{ve}/\sqrt{N_{pa}}$. As an example, a giant unilamellar vesicle of size 10 μm could engulf 100 nanoparticles of radius 100 nm, and its reduced volume would increase by less than 2%. Thus, for sufficiently small nanoparticles, we can ignore the tiny changes in the overall vesicle shape and identify the mean curvature M'_{ms} in eq 3 with the mean curvature M_{ms} in eq 2. This approximation is justified as long as the overall vesicle shape stays on the same branch of equilibrium shapes as the reduced volume is increased from v to v', that is, unless the vesicle undergoes a shape transition (see Figure 4 below). Furthermore, the relevant properties of the nanoparticles are encoded in the contact mean curvature M_{co} as defined byeq 1). Therefore, the nanoparticle–vesicle morphologies are now determined by only three parameters, namely v, m, and M_{co} (measured in units of $1/R_{ve}$).

Now, consider a certain vesicle shape as determined by v and m. Unless the vesicle is perfectly spherical, which corresponds to the limit case $v = 1$, the mean curvature M_{ms} will vary along the vesicle membrane in a continuous fashion. As a consequence, such a vesicle will display all membrane curvatures in the closed interval $M^{min}_{v,m} \le M_{ms} \le M^{max}_{v,m}$, where $M^{min}_{v,m}$ and $M^{max}_{v,m}$ are the minimal and maximal membrane curvatures of the vesicle. Using the inequalities described above that define the different stability regimes, it is now straightforward to determine which types of membrane segments will be present on a given vesicle. The general procedure is illustrated in Figure 2. A given vesicle can be

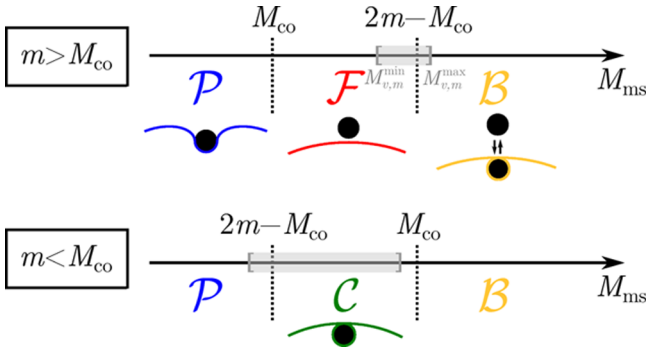

Figure 2. Engulfment regimes $\mathcal{P}$, $\mathcal{B}$, $\mathcal{F}$, or $\mathcal{C}$ as a function of membrane segment curvature M_{ms}: The possible regimes depend on whether the spontaneous curvature m exceeds the contact mean curvature M_{co} (top row) or vice versa (bottom row). The boundaries between the different regimes follow from the stability limits $M_{ms} = M_{co}$ and $M_{ms} = 2m - M_{co}$. For a given shape of the vesicle, all segment curvatures are located within a closed interval $M^{min}_{v,m} \le M_{ms} \le M^{max}_{v,m}$, as illustrated by the two shaded rectangles. For $m = 0$, these shaded intervals correspond to a prolate (top) and a stomatocyte (bottom), see Figure 4.

represented by the closed interval $M^{min}_{v,m} \le M_{ms} \le M^{max}_{v,m}$. The M_{ms}-axis is divided up into three nonoverlapping intervals by the two stability limits $M_{ms} = M_{co}$ and $M_{ms} = 2m - M_{co}$. It then follows that not all combinations of different engulfment regimes or *engulfment patterns* can be found on the same vesicle. For the case $m > M_{co}$, we find six possible patterns: three single-segment patterns with the whole vesicle being composed of a $\mathcal{P}$, $\mathcal{F}$, or $\mathcal{B}$ segment, two two-segment patterns with coexistence of $\mathcal{F} + \mathcal{P}$ or $\mathcal{F} + \mathcal{B}$ segments, and one three-segment pattern of coexisting $\mathcal{F} + \mathcal{B} + \mathcal{P}$ segments. For the case $m < M_{co}$, we find again the single-segment $\mathcal{P}$ and $\mathcal{B}$ patterns, plus four new possible patterns: a single-segment $\mathcal{C}$ pattern, two two-segment patterns $\mathcal{P} + \mathcal{C}$ and $\mathcal{B} + \mathcal{C}$, and one three-segment pattern $\mathcal{B} + \mathcal{P} + \mathcal{C}$. Thus, in contrast to the naive expectation that the four different types of membrane segments might form $2^4 - 1 = 15$ different engulfment patterns, which represents the number of nonempty subsets of a set with four elements, we find that a vesicle can exhibit only ten such patterns: four single-segment patterns, four two-segment patterns, and two three-segment patterns. Furthermore, we can exclude the $\mathcal{P} + \mathcal{B}$ two-segment pattern (apart from the exceptional case $M_{co} = m$) and all patterns that contain both an $\mathcal{F}$ and a $\mathcal{C}$ segment, compare Figure 2.

We can now use this type of reasoning to quantitatively describe the engulfment patterns present on the equilibrium shapes of free vesicles, as a function of the three free parameters v, m, and M_{co}. In Figure 3, we illustrate the engulfment patterns

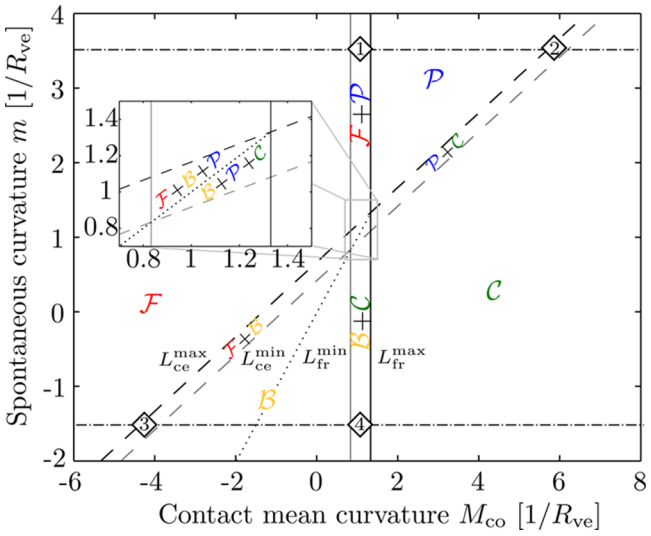

Figure 3. Engulfment patterns as a function of contact mean curvature M_{co} and spontaneous curvature m for a prolate vesicle with reduced volume $v = 0.98$. The solid vertical lines and the dashed tilted lines are given by the stability limits L^{min}_{fr}, L^{max}_{fr}, L^{min}_{ce}, and L^{max}_{ce}; see text. These four lines partition the (M_{co}, m) plane into the four extended regions $\mathcal{F}$, $\mathcal{B}$, $\mathcal{C}$, and $\mathcal{P}$, characterized by single-segment patterns, the four stripes $\mathcal{F} + \mathcal{B}$, $\mathcal{B} + \mathcal{C}$, $\mathcal{P} + \mathcal{C}$, and $\mathcal{F} + \mathcal{P}$, corresponding to two-segment patters, and the intersection region of the stripes. The latter region contains the two three-segment patterns $\mathcal{F} + \mathcal{B} + \mathcal{P}$ and $\mathcal{B} + \mathcal{P} + \mathcal{C}$, which are separated by the dotted line with $m = M_{co}$; see inset. The dotted line line also provides a very good approximation to the transition line at which the free and completely engulfed states switch metastability in the bistable $\mathcal{B}$ region. The horizontal dotted-dashed lines and the numbered diamonds refer to Figure 1.

as a function of spontaneous curvature m and contact mean curvature M_{co} for a prolate vesicle with reduced volume $v = 0.98$. The different engulfment patterns are separated from each other by the four lines L^{min}_{fr}, L^{max}_{fr}, L^{min}_{ce}, and L^{max}_{ce}, corresponding to the stability limits L_{fr} and L_{ce}, as given by eqs 2 and 3, for the membrane segments of minimal and maximal curvature of the vesicle $M_{ms} = M^{min}_{v,m}$ and $M^{max}_{v,m}$. In this case, the four lines appear essentially straight because the overall shape of the vesicle

DOI: 10.1021/acs.nanolett.5b03475
Nano Lett. 2015, 15, 7168–7173

hardly changes as we vary the spontaneous curvature m over the range displayed in Figure 3. In addition, the line $M_{co} = m$ separates the two three-segment patterns $\mathcal{F} + \mathcal{B} + \mathcal{P}$ and $\mathcal{B} + \mathcal{P} + C$, and provides a very good approximation to the transition line at which the free and completely engulfed states of the particle switch their metastability in the bistable $\mathcal{B}$ region. Large positive values of m lead to single-segment patterns with partially engulfed states. In contrast, negative values of m increase the stability of completely engulfed states and enhance the bistability of the system, which may be used to reversibly load and release the nanoparticles in response to external forces. The horizontal dotted−dashed lines and the numbered diamonds refer to Figure 1, and represent the evolution of the engulfment patterns as a function of increasing particle size or adhesiveness. As seen in Figure 1a, partial engulfment is more persistent at the weakly curved equator of the prolate vesicle. As the contact curvature increases and we cross the vertical line L_{fr}^{min} in Figure 3, a $\mathcal{P}$ segment starts to grow continuously from the equator until it covers the whole vesicle when we reach the L_{fr}^{max} line. The $\mathcal{P}$ segment only starts to shrink once we cross the L_{ce}^{max} line, and disappears at the equator when we cross the line L_{ce}^{min}, the vesicle being now covered by a single C segment. In contrast, bistable behavior is favored at the strongly curved poles of the vesicle, from which the $\mathcal{B}$ segments start to grow and then shrink; see Figure 1b.

In Figure 3, which applies to reduced volume $v = 0.98$, the parameter regions with stable two- or three-segment patterns are relatively small and, thus, require fine-tuning of the parameters M_{co} and m. Multisegment patterns, on the other hand, become more and more frequent as we decrease the reduced volume v and, thus, increase the difference between $M_{v,m}^{min}$ and $M_{v,m}^{max}$. This tendency is illustrated in Figure 4, which displays the engulfment patterns as a function of reduced volume v and contact mean curvature M_{co} for vesicles with spontaneous curvature $m = 0$. As the reduced volume v is decreased by osmotic deflation, the vesicle undergoes two morphological transitions, from prolates to discocytes and from discocytes to stomatocytes,[20] corresponding to the two horizontal lines in Figure 4. For the prolate branch, the two-segment regions rapidly expand as the vesicle is deflated from a sphere. For the discocyte and stomatocyte branches, one finds large regions of the parameter space with stable three-segment patterns. In these regions, partial engulfment is again favored at the segments of lowest membrane curvature, such as at the poles of the discocyte and at the central invagination of the stomatocyte, whereas bistability occurs in the segments of highest membrane curvature. Moving vertically along this engulfment pattern diagram can be easily accomplished experimentally, by simply changing the reduced volume via osmotic deflation and inflation.

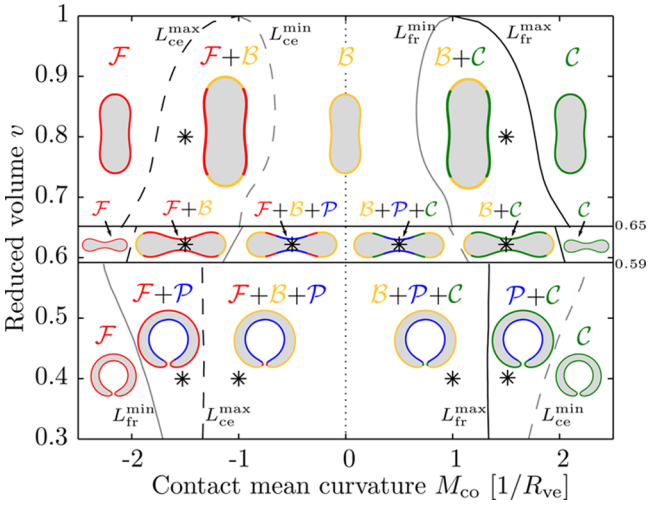

Figure 4. Engulfment patterns as a function of contact mean curvature M_{co} and reduced volume v for spontaneous curvature $m = 0$. The four lines L_{fr}^{min}, L_{fr}^{max}, and L_{ce}^{min}, and L_{ce}^{max} are now highly curved, compare to Figure 3, and are discontinuous along the two solid horizontal lines, which represent shape transitions of the free vesicle. The asterisks indicate the precise positions of the displayed 2-segment and 3-segment patterns.

In order to obtain the stability regimes for nanoparticles originating from the *interior* aqueous compartment, we must replace R_{pa} by $-R_{pa}$ in the expression 1 for the contact mean curvature M_{co}, which now decreases for increasing particle size R_{pa} or adhesive strength $|W|$. The inequalities that define the different segment types then change sign, which implies that the stability regimes in Figures 2, 3, and 4 are swapped according to $\mathcal{F} \leftrightarrow C$ and $\mathcal{B} \leftrightarrow \mathcal{P}$. In contrast to the endocytic case, positive spontaneous curvatures and small segment curvatures now enhance bistability, whereas negative spontaneous curvatures and large segment curvatures promote partial engulfment.

In this Letter, we focused on the membrane−particle interactions and ignored possible particle−particle interactions mediated by the membrane. The latter interactions are obviously absent for the $\mathcal{F}$ segments but should also play no role for $\mathcal{B}$ and C segments because, in the completely engulfed state, the membrane experiences only a local, point-like deformation at the position of the neck, which costs no energy. Thus, completely engulfed particles are unable to "feel" each other and are expected to diffuse freely on the $\mathcal{B}$ and C segments. On the other hand, if a completely engulfed particle diffuses from a $\mathcal{B}$ or C segment into an $\mathcal{F}$ or $\mathcal{P}$ segment, it will unbind or partially unwrap from the membrane. The partially engulfed particles within $\mathcal{P}$ segments may "feel" local curvature gradients and can then aggregate into particle clusters.[5,29,30] However, such a clustering process does not affect the distinction between the $\mathcal{F}$, $\mathcal{B}$, C, and $\mathcal{P}$ segments and, thus, does not change the engulfment patterns described above.

The engulfment patterns described here should be directly observable in the optical microscope using fluorescently labeled particles. For a membrane with known bending rigidity, the mean contact curvature can be tuned by using nanoparticles of an appropriate material and size. As an example, the adhesive strength between DMPC bilayers and silica was measured[31] to be on the order of $|W| \simeq 0.5$ mJ/m^2. Using eq 1 and the measured value[32] of the bending rigidity $\kappa \simeq 18\ k_BT$ for DMPC bilayers, we see that the contact mean curvature can be varied from $M_{co} \simeq -1/(75\text{ nm})$ to $+1/(79\text{ nm})$ as we increase the nanoparticle size from $R_{pa} = 14$ to 22 nm. In addition, the adhesive strength and thus the contact mean curvature may be tuned in a continuous manner by changing the salt concentration of the aqueous solution.[8] Furthermore, the spontaneous curvature of the membrane can be varied over a wide range from $|m| \sim 1/(100\ \mu\text{m})$ to $1/(20\text{ nm})$ via asymmetric adsorption of ions, small molecules or larger polymers and proteins,[33,34] as well as through the controlled formation of bilayers with compositional asymmetry.[35−37] Finally, the reduced volume and therefore the vesicle shape can be controlled using osmotic deflation and inflation.

DOI: 10.1021/acs.nanolett.5b03475
Nano Lett. 2015, 15, 7168−7173

We have shown that the nonaxisymmetric configurations of nanoparticles and membranes can be studied by local stability analysis, as embodied in the two stability relations (eqs 2 and eq 3). These relations depend on two material parameters: the contact mean curvature M_{co} as given by eq 1, and the spontaneous curvature m, and imply four distinct types of stable membrane segments. As a consequence, a nanoparticle will be either free, partially engulfed, completely engulfed, or show bistability between partially and completely engulfed states, depending on the local curvature of the membrane. For small particle radii, the stability relations can be used to predict ten distinct engulfment patterns on complex membrane shapes as provided, for example, by prolate, discocyte, or stomatocyte vesicles as well as morphological transitions between these patterns, see Figures 1−4. These patterns should be directly observable in the optical microscope using fluorescently labeled particles.

The stability relations (eqs 2 and 3) have been derived for the spontaneous curvature model in ref 14 but should have the same form in the area-difference-elasticity model.[38] The latter model describes bilayer membranes for which one can ignore molecular flip-flops between the two leaflets of the bilayers and, thus, assume that each leaflet has a fixed number of molecules irrespective of the membrane shape. For this model, the stability relations (eqs 2 and 3) should again hold provided one replaces the spontaneous curvature m by the effective spontaneous curvature $m_{\mathrm{eff}} \equiv m - \zeta/(4R_{ve})$ with $\zeta \sim R_{pa}/R_{ve}$. [The dimensionless quantity ζ is equal to $(\bar{\kappa}/\kappa)(q - q_0)$ where $\bar{\kappa}$ is the second bending rigidity of the area-difference-elasiticity model[38] with $\bar{\kappa}/\kappa \simeq 1$ and q denotes the integrated mean curvature $q \equiv \int \mathrm{d}A M/R_{ve}$, which attains the value q_0 for the relaxed vesicle shape with an optimal packing of the molecules in both leaflets. When the latter shape is quasispherical, one finds $q - q_0 \approx \pm 4\pi R_{pa}/R_{ve}$ for small size ratios R_{pa}/R_{ve} where the plus and minus sign apply to exo- and endocytosis, respectively. Note that $q - q_0$ has a fixed value for a given vesicle shape.] For the systems considered here, the size R_{pa} of the nanoparticles was taken to be much smaller than the size R_{ve} of the vesicles which implies that the effective spontaneous curvature m_{eff} is approximately equal to the spontaneous curvature m even in the absence of flip-flops between the bilayer leaflets.

In the present study, we focused on the engulfment patterns of free vesicles exposed to a single species of nanoparticles in order to demonstrate the far-reaching consequences of the stability relations (eqs 2 and 3). Because of their local nature, these relations can be generalized to more complex membrane systems. Relatively simple examples are provided by (i) binary mixtures of two nanoparticles with different sizes and (ii) vesicle membranes with coexisting membrane domains formed by liquid-ordered and liquid-disordered phases. In case (i), the two particle sizes lead to two different engulfment patterns which are superimposed on the vesicles. In case (ii), the different fluid−elastic parameters of the two membrane phases lead to coexisting engulfment patterns that are confined to the two types of membrane domains. Furthermore, we may consider vesicles that experience external forces or constraints arising, for example, from adhesive surfaces, micropipettes, or optical tweezers. In the latter cases, the stability relations (eqs 2 and 3) remain valid for the "unperturbed" membrane segments, that is, for those membrane segments that are neither in contact with other surfaces nor directly exposed to localized external forces. For the "perturbed" segments, on the other hand, we can derive generalized stability relations as will be shown in a subsequent paper. Finally, it will be rather interesting to study the engulfment patterns of cellular membranes. The shape of these membranes is often strikingly similar to the shape of vesicles but the particle engulfment usually involves additional processes such as the formation of protein coats in receptor-mediated endocytosis[14] or localized forces arising from the coupling to the cytoskeleton.

AUTHOR INFORMATION

Corresponding Author

*E-mail: lipowsky@mpikg.mpg.de.

Notes

The authors declare no competing financial interest.

ACKNOWLEDGMENTS

This study was supported by the German Research Foundation (DFG) via the IRTG 1524.

REFERENCES

(1) Petros, R. A.; DeSimone, J. M. *Nat. Rev. Drug Discovery* **2010**, *9*, 615−627.
(2) Rodriguez, P. L.; Harada, T.; Christian, D. A.; Pantano, D. A.; Tsai, R. K.; Discher, D. E. *Science* **2013**, *339*, 971−975.
(3) Lipowsky, R.; Döbereiner, H.-G. *Europhys. Lett.* **1998**, *43*, 219−225.
(4) Dietrich, C.; Angelova, M.; Pouligny, B. *J. Phys. II* **1997**, *7*, 1651−1682.
(5) Koltover, I.; Rädler, J.; Safinya, C. *Phys. Rev. Lett.* **1999**, *82*, 1991−1994.
(6) Fery, A.; Moya, S.; Puech, P. H.; Brochard-Wyart, F.; Mohwald, H. *C. R. Phys.* **2003**, *4*, 259−264.
(7) Michel, R.; Kesselman, E.; Plostica, T.; Danino, D.; Gradzielski, M. *Angew. Chem., Int. Ed.* **2014**, *53*, 12441−12445.
(8) Strobl, F. G.; Seitz, F.; Westerhausen, C.; Reller, A.; Torrano, A. A.; Bräuchle, C.; Wixforth, A.; Schneider, M. F. *Beilstein J. Nanotechnol.* **2014**, *5*, 2468−2478.
(9) Jaskiewicz, K.; Larsen, A.; Schaeffel, D.; Koynov, K.; Lieberwirth, I.; Fytas, G.; Landfester, K.; Kroeger, A. *ACS Nano* **2012**, *6*, 7254−7262.
(10) Deserno, M. *Phys. Rev. E* **2004**, *69*, 031903.
(11) Góźdź, W. T. *Langmuir* **2007**, *23*, 5665−5669.
(12) Nowak, S. A.; Chou, T. *Phys. Rev. E* **2008**, *78*, 021908.
(13) Cao, S.; Wei, G.; Chen, J. Z. Y. *Phys. Rev. E* **2011**, *84*, 050901.
(14) Agudo-Canalejo, J.; Lipowsky, R. *ACS Nano* **2015**, *9*, 3704−3720.
(15) Yi, X.; Shi, X.; Gao, H. *Nano Lett.* **2014**, *14*, 1049−1055.
(16) Dasgupta, S.; Auth, T.; Gompper, G. *Nano Lett.* **2014**, *14*, 687−693.
(17) Vácha, R.; Martinez-Veracoechea, F. J.; Frenkel, D. *Nano Lett.* **2011**, *11*, 5391−5395.
(18) Huang, C.; Zhang, Y.; Yuan, H.; Gao, H.; Zhang, S. *Nano Lett.* **2013**, *13*, 4546−4550.
(19) Lipowsky, R. *Nature* **1991**, *349*, 475−481.
(20) Seifert, U.; Berndl, K.; Lipowsky, R. *Phys. Rev. A: At., Mol., Opt. Phys.* **1991**, *44*, 1182−1202.
(21) Voeltz, G. K.; Prinz, W. A. *Nat. Rev. Mol. Cell Biol.* **2007**, *8*, 258−264.
(22) Shibata, Y.; Hu, J.; Kozlov, M. M.; Rapoport, T. A. *Annu. Rev. Cell Dev. Biol.* **2009**, *25*, 329−354.
(23) Terasaki, M.; Shemesh, T.; Kasthuri, N.; Klemm, R. W.; Schalek, R.; Hayworth, K. J.; Hand, A. R.; Yankova, M.; Huber, G.; Lichtman, J. W.; Rapoport, T. A.; Kozlov, M. M. *Cell* **2013**, *154*, 285−296.

DOI: 10.1021/acs.nanolett.5b03475
Nano Lett. 2015, 15, 7168−7173

(24) Kim, K. T.; Zhu, J.; Meeuwissen, S. A.; Cornelissen, J. J. L. M.; Pochan, D. J.; Nolte, R. J. M.; Van Hest, J. C. M. *J. Am. Chem. Soc.* **2010**, *132*, 12522−12524.
(25) Jülicher, F.; Seifert, U.; Lipowsky, R. *Phys. Rev. Lett.* **1993**, *71*, 452−455.
(26) Michalet, X.; Bensimon, D. *Science* **1995**, *269*, 666−668.
(27) Helfrich, W. *Z. Naturforsch. C* **1973**, *28*, 693−703.
(28) Seifert, U.; Lipowsky, R. *Phys. Rev. A: At., Mol., Opt. Phys.* **1990**, *42*, 4768−4771.
(29) Bahrami, A. H.; Lipowsky, R.; Weikl, T. R. *Phys. Rev. Lett.* **2012**, *109*, 188102.
(30) Šarić, A.; Cacciuto, A. *Phys. Rev. Lett.* **2012**, *109*, 188101.
(31) Anderson, T. H.; Min, Y.; Weirich, K. L.; Zeng, H.; Fygenson, D.; Israelachvili, J. N. *Langmuir* **2009**, *25*, 6997−7005.
(32) Brüning, B. A.; Prévost, S.; Stehle, R.; Steitz, R.; Falus, P.; Farago, B.; Hellweg, T. *Biochim. Biophys. Acta, Biomembr.* **2014**, *1838*, 2412−2419.
(33) Lipowsky, R. *Faraday Discuss.* **2013**, *161*, 305−331.
(34) Różycki, B.; Lipowsky, R. *J. Chem. Phys.* **2015**, *142*, 054101.
(35) Hu, P. C.; Li, S.; Malmstadt, N. *ACS Appl. Mater. Interfaces* **2011**, *3*, 1434−1440.
(36) Richmond, D. L.; Schmid, E. M.; Martens, S.; Stachowiak, J. C.; Liska, N.; Fletcher, D. A. *Proc. Natl. Acad. Sci. U. S. A.* **2011**, *108*, 9431−9436.
(37) Matosevic, S.; Paegel, B. M. *Nat. Chem.* **2013**, *5*, 958−963.
(38) Miao, L.; Seifert, U.; Wortis, M.; Döbereiner, H.-G. *Phys. Rev. E: Stat. Phys., Plasmas, Fluids, Relat. Interdiscip. Top.* **1994**, *49*, 5389−5407.

DOI: 10.1021/acs.nanolett.5b03475
Nano Lett. 2015, 15, 7168−7173